

## RADIOCARBON

CAMBRIDGE  
UNIVERSITY PRESS**Forecasting atmospheric radiocarbon decline to pre-bomb  
values**

Journal:	<i>Radiocarbon</i>
Manuscript ID	RDC-ENVI-2017-0053
Manuscript Type:	2017 C-14 in Environment Conf. Paper
Date Submitted by the Author:	15-Jul-2017
Complete List of Authors:	Sierra, Carlos; Max-Planck-Institut fur Biogeochemie, Biogeochemical Processes
Keywords:	Cities, Bomb curve, Time series decomposition, Fossil fuels, Statistical forecast

SCHOLARONE™  
Manuscripts

1    **Forecasting atmospheric radiocarbon**  
2    **decline to pre-bomb values**

3                                    Carlos A. Sierra

4    **Affiliation:**

5    *Max Planck Institute for Biogeochemistry, Jena, Germany*

7    **Correspondence:**

8    Max-Planck-Institute for Biogeochemistry, Hans-Knöll-Str. 10, 07745 Jena,  
9    Germany. Phone: +49 3641 576133, fax: +49 3641 577100, email: csierra@bgc-  
10    jena.mpg.de.

## Abstract

In this manuscript, I present an estimation of the rate of decline in atmospheric radiocarbon and the amplitude of its seasonal cycle for the past four decades for the northern and southern hemispheres, and forecast the time required to reach pre-1950 levels (i.e.  $\Delta^{14}\text{C} < 0\text{‰}$ ). Using a set of 30 different exponential smoothing state-space models, the time series were decomposed into their error, trend, and seasonal components, choosing the model that best represented the observed data. According to the best model, the rate of change in  $\Delta^{14}\text{C}$  has decreased considerably since the 1970s and stabilized recently between -2.4 and -2.6 ‰ per year. Overall, the time-series showed larger rates of radiocarbon decline in the northern than in the southern hemisphere, and relatively stable seasonal cycles for both hemispheres. A forecast of the exponential smoothing models predicts that radiocarbon concentrations will reach pre-1950 levels by 2030 in the northern hemisphere with 20% probability, and by around 2040 in the southern hemisphere. However, at regional levels radiocarbon concentrations have already reached pre-1950 levels in several industrialized regions and cities around the world as a consequence of fossil-fuel emissions.

**Keywords:** Time series decomposition, bomb curve, fossil fuels, cities, statistical forecast.

32 **1 Introduction**

33 In the early 1950s Hans Suess described a significant decrease in radiocarbon  
34 concentrations in the atmosphere due to the combustion of fossil fuels, which  
35 contain virtually no radiocarbon and therefore dilute atmospheric  $^{14}\text{C}$  relative  
36 to  $^{12}\text{C}$  (Suess, 1953, 1955). This trend changed dramatically in the late 1950s  
37 and early 1960s when nuclear-bomb tests increased atmospheric radiocarbon  
38 concentrations to levels not ever seen before in the last 50,000 years of Earth's  
39 history. Since then, radiocarbon concentrations have been declining globally  
40 as evidenced by data from tree-rings and more recent direct atmospheric  
41 observations (Tans et al., 1979; Manning et al., 1990; Levin et al., 1989;  
42 Currie et al., 2011; Graven et al., 2012; Hua et al., 2013; Levin et al., 2013).

43 Using a simple box model of the global carbon cycle, Caldeira et al. (1998)  
44 predicted that atmospheric radiocarbon concentrations will continue a neg-  
45 ative rate of decline until the beginning of the 21st century and will return  
46 to pre-1950 values around the year 2020. More recently, Graven (2015) pre-  
47 dicted a similar time for returning to pre-1950s values, but with different  
48 trajectories according to different fossil-fuel emission scenarios. This point,  
49 where  $\Delta^{14}\text{C}$  values go from positive to negative, indicate a transition where  
50 fossil-fuel derived  $\text{CO}_2$  dominates the atmospheric signal of radiocarbon, pre-  
51 viously dominated by bomb-derived radiocarbon.

52 Determining this transition point in atmospheric radiocarbon is impor-  
53 tant for different reasons. For instance, a) it helps to determine the impact of  
54 fossil fuel emissions on the global carbon cycle (Caldeira et al., 1998; Turnbull  
55 et al., 2009; Graven, 2015), b) it serves as an important benchmark for global

carbon models since the rate of radiocarbon decline is the result of different processes rates in global C reservoirs, and appropriate representation of these processes in models must predict accurately this transition point (Oeschger et al., 1975; Randerson et al., 2002; Naegler and Levin, 2006), and d) it sets a new reference point for dating organic material of interest in biology, biogeochemistry, and archeology (Graven, 2015).

Post-bomb atmospheric radiocarbon data for different hemispheric zones have been compiled and homogenized by Hua et al. (2013), harmonizing measurements from tree-rings (e.g. Hertelendi and Csongor, 1983; Levin and Kromer, 1997; Hua et al., 2000; Park et al., 2002; Yamada et al., 2005; Hua et al., 2012; Rakowski et al., 2013) and direct atmospheric observations (e.g. Vogel and Marais, 1971; Berger et al., 1987; Manning et al., 1990; Nydal and Loevseth, 1996; Levin and Kromer, 2004; Meijer et al., 2006; Turnbull et al., 2007; Levin et al., 2010; Currie et al., 2011; Graven et al., 2012) (Figure 1). These hemispheric ‘bomb curves’ contain very useful information on the trend and seasonality of atmospheric radiocarbon for different hemispheric regions. Furthermore, this information can be used to forecast future trends in atmospheric radiocarbon and determine the possible transition date to pre-1950 levels.

Standard atmospheric radiocarbon curves are only released to the scientific community at irregular intervals (Hua and Barbetti, 2004; Hua et al., 2013), and there is a need to produce forecasts of these curves for periods not covered by the standard curves. For instance, radiocarbon dating methods or analyses of cycling rates in carbon reservoirs using samples from recently collected material require best estimates of the atmospheric radiocarbon values

81 for time intervals after the latests release of the standard radiocarbon curves  
 82 (Sierra et al., 2014) . For this reason, it is important to provide robust  
 83 statistical methods for forecasting that can provide accurate predictions.

84 Here I present a time-series decomposition analysis for the atmospheric  
 85 radiocarbon curves of Hua et al. (2013), fitting a set of exponential smoothing  
 86 state-space models with the aim to forecast future trends in radiocarbon at  
 87 hemispheric scales. The main objectives of this analysis are, a) to decompose  
 88 the observed time series into trend and seasonal components and characterize  
 89 differences among hemispheric zones, and b) to identify the probability of  
 90 returning to pre-bomb radiocarbon values; i.e.  $\Delta^{14}\text{C} \leq 0\%$ . Additionally, I  
 91 present radiocarbon measurements of plants from different cities to identify  
 92 the degree at which, by local dilution, atmospheric radiocarbon has already  
 93 crossed this threshold.

## 94 2 Methods

### 95 2.1 Time series decomposition

96 I used the harmonized atmospheric radiocarbon time series reported by Hua  
 97 et al. (2013) for the northern and southern hemispheres. Although these  
 98 authors present curves for four different hemispheric zones, the curves only  
 99 deviate from each other during the early bomb period. Here, I use data from  
 100 the year 1975 to 2010, where intra-hemispheric differences are not reported,  
 101 and only the northern and the southern hemispheres are differentiated.

102 These hemispheric radiocarbon time-series are not available at regularly

103 spaced intervals as required by the time-series analysis used here; therefore,  
 104 they were homogenized in regular monthly and seasonal periods by cubic  
 105 spline interpolation (Figure 1b).

106 To analyze each time series, I used the ETS framework described by  
 107 Hyndman et al. (2008) to fit 30 different exponential smoothing state-space  
 108 models that decompose the series in the error (E), trend (T), and seasonal  
 109 (S) components (ETS decomposition). In classical time-series decomposi-  
 110 tion methods, trend, seasonality and error are commonly assumed as linear  
 111 additive terms (e.g. Cleveland et al., 1983), which in the ETS framework im-  
 112 ply a model of the form  $E+T+S$ . However, many other methods have been  
 113 proposed to decomposed time series in its inherent components, not only  
 114 considering linear additive models. For instance, models can have all terms  
 115 multiplicative ( $E*T*S$ ), or combinations between additive and multiplicative  
 116 terms (e.g.  $E*T+S$ ). The different combinations of potential model struc-  
 117 tures results in the 30 different models tested here. As selection criterion, I  
 118 used the Akaike information criterion (AIC), which selects the best model ac-  
 119 cording to goodness of fit and the complexity of the model, given preference  
 120 to the simplest model that can best predict the observations.

121 When the data contains zeros or negative values, the multiplicative error  
 122 models in the ETS framework are not numerically stable (Hyndman et al.,  
 123 2008). For this reason, I used the radiocarbon series as fraction modern  $F$  in  
 124 all computations, using the relation  $\Delta^{14}\text{C} = (F - 1) \cdot 1000$  to convert among  
 125 different reporting conventions (Reimer et al., 2004).

126 ETS models predict observations  $y_t$  according to a function of the error,  
 127 trend, and seasonal components  $f(E, T, S)$ . The trend component is also

split between a level  $l$  and a growth term  $b$ . The error term  $\varepsilon$  is considered a Gaussian white-noise process with variance  $\sigma^2$ . The mean value of the observations is therefore predicted by a function

$$\mu_t = f(\varepsilon, l, b, s, \theta), \quad (1)$$

where  $\theta$  are a set of parameters that weigh the contributions from the different components. Parameter estimation is performed by maximum likelihood.

Forecasting is performed by recursively applying the ETS model  $h$  number of steps ahead the last observation. Specific details about the method and its implementation in the R package `forecast` are provided in Hyndman et al. (2008) and Hyndman and Khandakar (2008), respectively. In the supplementary material I provide all code necessary to reproduce the results presented here.

## 2.2 Radiocarbon in local air

I also used radiocarbon analyses in organic material from annual plants to infer the atmospheric radiocarbon concentration in a set of cities around the world. Annual plants incorporate local sources of carbon dioxide during the growing season, providing an integrated measure of the radiocarbon concentration of the local air (Hsueh et al., 2007). For consistency, I sampled at each location at least three individuals of dandelion (*Taraxacum spp.*), an annual plant that can be found growing in most cities. For comparison, I also sampled plants at locations with low influence of anthropogenic fossil fuel emissions such as the Rocky Mountain National Park (RMNP) in the



149 USA, the Austrian Alps, and in the Amazon basin at the town of Leticia,  
 150 Colombia. Plants were washed and air-dried after sampling to eliminate con-  
 151 tamination from dust and other particles. All samples were then oven-dried  
 152 at 70° Celsius and ground in a ball-grinder at the Max Planck Institute for  
 153 Biogeochemistry in Jena, Germany. Radiocarbon analyses were conducted  
 154 by Accelerator Mass Spectrometry at the same institution (Steinhof et al.,  
 155 2004).

## 156 **3 Results**

### 157 **3.1 Time series decomposition**

158 From the 30 different competing models, the best performance was obtained  
 159 by an ETS model of the form: (M,A,M), which means that the error and the  
 160 seasonal terms are multiplicative, and the trend term is additive. Specifically,  
 161 for both hemispheric curves the model with the best AIC had the form:

$$\begin{aligned}\mu_t &= (l_{t-1} + b_{t-1})s_{t-m}, \\ l_t &= (l_{t-1} + b_{t-1})(1 + \alpha\varepsilon_t), \\ b_t &= b_{t-1} + \beta(l_{t-1} + b_{t-1})\varepsilon_t, \\ s_t &= s_{t-m}(1 + \gamma\varepsilon_t).\end{aligned}$$

162 For the northern hemisphere time series, the value of the parameters were  
 163  $\theta_{NH} : (\alpha = 0.75, \beta = 0.03, \gamma = 0.0001)$ ; and for the southern hemisphere

$\theta_{SH} : (\alpha = 0.23, \beta = 0.008, \gamma = 0.0001)$ . Notice that the main differences among the two models are on the parameters  $\alpha$  and  $\beta$  that control the degree by which the error term influence the level and growth terms, respectively. This implies that for the northern hemisphere, the level and the growth terms showed more variability than in the southern hemispheres (Figure 2). The seasonal term has very little influence from the error term as predicted by  $\gamma$ , therefore the seasonal cycle obtained from this model has a very regular pattern.

The temporal pattern of the growth term  $b_t$  was relatively similar between the northern and the southern hemispheres (Figure 2), but the curve for the level term was always lower for the northern hemisphere, which results in a larger decline of atmospheric radiocarbon for the north. For the last year in both time series, the decline in atmospheric radiocarbon in  $\Delta^{14}\text{C}$ , calculated as the sum of the last 12  $b_t$  terms of the series, was -2.4 ‰ in the northern hemisphere, and -2.6 ‰ in the southern hemisphere.

Since the seasonal pattern is a multiplicative term centered around 1, the absolute amplitude of the seasonal cycle is predicted to decline in this model for both hemispheres, but proportionally to the actual radiocarbon concentration in the atmosphere. The lower the value of the trend  $(l + b)$  the lower the amplitude of the term  $\mu_t$ . The model predicts a higher influence of the seasonal term for the northern than for the southern hemisphere. The model also predicts, as previously reported (Levin et al., 2010; Currie et al., 2011), a reversed seasonality between the northern and the southern hemispheres (Figure 2c).

## 188 3.2 Forecast

189 A forecast of the atmospheric radiocarbon time series was obtained by ex-  
190 ponential smoothing of the ETS model, i.e. recursively applying the set  
191 of equations with the best parameter values found (Hyndman et al., 2008).  
192 The forecast was obtained on quarterly intervals and not on a monthly basis  
193 since the multiplicative error term strongly influences uncertainty bounds  
194 in predictions at short-time scales. This is a relatively well-known issue  
195 in forecasting methods (Athanasopoulos et al., 2017), and it is commonly  
196 recommended to produce forecasts at an intermediate time-scale such as ev-  
197 ery four months in long-term monthly time-series (Nijman and Palm, 1990;  
198 Rossana and Seater, 1995; Athanasopoulos et al., 2017).

199 For the two series, the forecast of the average radiocarbon values showed  
200 a linear decrease for the next 20 years (Figure 3). This linear decline is  
201 based on the observed stabilization of the growth term of the time series  
202 (Figure 2a). The range of the prediction intervals increases in all series  
203 because of the nature of the exponential smoothing model that assigns less  
204 weight to successively older observations and therefore the uncertainty in the  
205 predictions increases.

206 Atmospheric radiocarbon is predicted to decline faster in the northern  
207 hemisphere than in the southern hemisphere, therefore it is more likely that  
208 radiocarbon values return to pre-1950 values earlier in the northern hemi-  
209 sphere. Uncertainty ranges are also higher for the northern than for the  
210 southern hemisphere as a consequence of higher values of the parameters  $\alpha$   
211 and  $\beta$  from the ETS model.

212 Independent observations of atmospheric radiocarbon from European sta-  
213 tions at the Schauinsland and Jungfraujoch sites (Levin et al., 2013), are  
214 within forecast uncertainty range for the northern hemisphere (Figure 4a).  
215 The observations from these stations follow relatively well the forecasted  
216 seasonal cycle, however they are below the forecasted mean. One likely ex-  
217 planation for this difference, is the potential contribution of fossil-fuel derived  
218 carbon to these central European stations (Levin et al., 1989; Turnbull et al.,  
219 2009; Levin et al., 2013).

220 To predict the decline in atmospheric radiocarbon for central Europe  
221 based on the Jungfraujoch and Schauinsland stations, I ran a forecast se-  
222 lecting the ETS model that best matches the observations reported in Levin  
223 et al. (2013) (Figure 4b). In this forecast, the rate of radiocarbon decline is  
224 faster, and mean atmospheric radiocarbon crosses the  $\Delta^{14}\text{C} = 0\text{‰}$  threshold  
225 much earlier.

226 Atmospheric radiocarbon is expected to return to pre-1950s levels within  
227 the next decades with different probabilities for the different hemispheres.  
228 Values of  $\Delta^{14}\text{C} \leq 0\text{‰}$  are within 95% prediction intervals of the forecast  
229 starting as early as 2019 for the northern hemisphere, and 2029 for the south-  
230 ern hemisphere. For central Europe, it is very likely ( $> 90\%$  probability) that  
231 the  $\Delta^{14}\text{C} \leq 0\text{‰}$  threshold is being crossed by summer 2017.

232 Although the hemispheric averages of background air are expected to  
233 return to pre-1950 levels within the next decades, this threshold has been  
234 already crossed locally in major cities around the world (Figure 6). Air  
235 in metropolitan areas with high fossil-fuel emission levels such as Medellín,  
236 Stockholm, and the Newport Beach area in California show the highest in-

fluence of fossil-fuel derived carbon. Air in European cities such as Berlin and Prague had not crossed the pre-1950 level yet, but Jerusalem was in the limit in 2014 ( $-0.1 \pm 2.4$  ‰). As expected, the high altitude samples from the Austrian Alps are very close to the forecasted global values, whereas the samples from Rocky Mountain National Park were much below the forecasted global average, but within the 80% prediction intervals of the forecast.

## 4 Discussion

The time series decomposition presented here shows properties of the trend, slope, and seasonality of atmospheric radiocarbon for different hemispheric zones that complements previous analyses based on sets of individual stations (Levin et al., 2010; Graven et al., 2012; Levin et al., 2013) and global carbon models (Caldeira et al., 1998; Randerson et al., 2002; Turnbull et al., 2009; Levin et al., 2010; Graven, 2015). One main advantage of this analysis is the use of the harmonized series compiled by Hua et al. (2013), which provide a spatial average across the different stations from which atmospheric radiocarbon has been measured. The series also resolve issues of temporal gaps for the individual stations, and give a comprehensive overview of the dynamic behavior of atmospheric radiocarbon in background air during the past 40 years for the two hemispheres.

The series decomposition analyses showed that the overall decline of atmospheric radiocarbon was higher in the northern hemisphere than in the southern hemisphere. This is not surprising because the large levels of fossil-fuel emissions in the northern hemisphere are expected to significantly dilute

260 atmospheric radiocarbon (Levin et al., 1989, 2010; Turnbull et al., 2009;  
261 Graven et al., 2012). Rates of decline stabilized at  $\sim -2.4$  to  $-2.6\text{‰}$  per  
262 year, in the last part of the curve. This implies that if rates of decline con-  
263 tinue at a constant rate in the future, atmospheric radiocarbon would decline  
264 in a linear trend. Furthermore, these low rates of decline may pose challenges  
265 for detecting temporal trends in atmospheric radiocarbon given that the un-  
266 certainty in new generation AMS systems is between 3 to 2‰ (Synal et al.,  
267 2007; Wacker et al., 2010).

268 Atmospheric radiocarbon is expected to return to pre-1950 levels in the  
269 northern hemisphere by 2020, the year predicted by Caldeira et al. (1998),  
270 with a probability  $\sim 7\%$ . In the southern hemisphere however, it is unlikely  
271 that atmospheric radiocarbon reach values below 0 ‰ by 2020. Based on  
272 more recent observations from central Europe, the pre-1950 threshold may  
273 have been already crossed with high probability ( $>90\%$ ) by summer 2017.

274 It is not possible to attribute any particular process that may contribute  
275 to the observed trends in the data with this statistical approach. However,  
276 previous analyses (Caldeira et al., 1998; Randerson et al., 2002; Levin et al.,  
277 2013; Currie et al., 2011) may help to explain some of the properties of  
278 the observed time series. For instance, different processes are responsible  
279 for determining atmospheric radiocarbon concentrations: fossil fuel emis-  
280 sions, ocean-atmosphere exchange, stratosphere-troposphere mixing, terres-  
281 trial ecosystem fluxes, emissions from nuclear industry, and cosmogenic pro-  
282 duction (Oeschger et al., 1975; Randerson et al., 2002; Naegler and Levin,  
283 2006; Levin et al., 2010; Graven, 2015). The recent slower rates of decline  
284 in the northern hemisphere may be explained by the contribution of the ter-

restrial biosphere and oceans that return decades-old bomb radiocarbon and therefore counterbalance the effect of increased fossil fuel emissions (Caldeira et al., 1998; Randerson et al., 2002; Currie et al., 2011). For the southern hemisphere, ocean-atmosphere exchange plays a larger role, and the slow in radiocarbon decline in recent years may be explained by return of bomb radiocarbon by the mixed layer (Currie et al., 2011).

The combined effect of terrestrial biosphere, ocean exchange, fossil-fuel emissions as well as horizontal and vertical air transport may have an important contribution in reducing the amplitude of the seasonal cycle (Levin et al., 2010). The best ETS model identified here, predicts the seasonal cycle as proportional to the trend term; i.e. the higher the amount of radiocarbon in the atmosphere the higher the amplitude of the seasonal cycle, and as radiocarbon concentrations decline in both hemispheres so does its seasonality. Given that the growth term of the series had stabilized in the recent decade, the amplitude of the seasonal cycle had remained constant in the last part of the curve. These results are consistent with model predictions by Randerson et al. (2002), who predicted a decline in seasonality over time due to decrease in seasonality in ocean and terrestrial biosphere exchange, with strong contributions from fossil-fuel signals.

Caldeira et al. (1998), and more recently Graven (2015), predicted that in a business-as-usual scenario of fossil-fuel emissions, radiocarbon concentrations would return to pre-1950 levels by  $\sim 2020$ . Current trajectories of atmospheric radiocarbon seem to agree with this prediction, but with important differences among hemispheric regions. The  $\Delta^{14}\text{C} \leq 0\text{‰}$  threshold would be crossed in the northern hemisphere with higher probability than

310 in the southern hemisphere, which may be a consequence of differences in  
311 contributions between the terrestrial biosphere and the oceans, the later be-  
312 ing more relevant for the southern hemisphere. It is also likely that the rate  
313 of decline of atmospheric radiocarbon in the northern hemisphere may in-  
314 crease in the future (become more negative) if the previously sequestered  
315 bomb-radiocarbon is exhausted, and then fossil-fuel radiocarbon may have a  
316 larger influence in the northern hemisphere. This is clearly illustrated in the  
317 urban areas we analyzed where fossil-fuel emissions dominate over terrestrial  
318 exchange and therefore radiocarbon is close or have already crossed the  $\Delta^{14}\text{C}$   
319  $\leq 0\text{‰}$  threshold.

320 The forecasted atmospheric radiocarbon curves presented here may be  
321 useful for different studies where data on the atmospheric background is not  
322 available after the latest release of the standard curves (Hua et al., 2013).  
323 The methodology of time-series decomposition and forecast may also be use-  
324 ful to produce forecasts for individual stations or for new releases of standard  
325 curves. However, care must be taken in using these forecasts in different ap-  
326 plications, and prediction uncertainties must always be considered. Possible  
327 changes in the rates of decline of atmospheric radiocarbon for the different  
328 hemispheres may deviate in the future from the rates calculated in the time-  
329 series decomposition presented here. Therefore, these forecasted radiocarbon  
330 trends must be used with caution.



## References

- Athanasopoulos, G., Hyndman, R. J., Kourentzes, N., and Petropoulos, F. (2017). Forecasting with temporal hierarchies. *European Journal of Operational Research*, 262(1):60 – 74.
- Berger, R., Jackson, T. B., Michael, R., and Suess, H. E. (1987). Radiocarbon content of tropospheric CO<sub>2</sub> at China Lake, California 1977–1983. *Radiocarbon*, 29(1):18–23.
- Caldeira, K., Rau, G. H., and Duffy, P. B. (1998). Predicted net efflux of radiocarbon from the ocean and increase in atmospheric radiocarbon content. *Geophysical Research Letters*, 25(20):3811–3814.
- Cleveland, W. S., Freney, A. E., and Graedel, T. E. (1983). The seasonal component of atmospheric CO<sub>2</sub>: Information from new approaches to the decomposition of seasonal time series. *Journal of Geophysical Research: Oceans*, 88(C15):10934–10946.
- Currie, K. I., Brailsford, G., Nichol, S., Gomez, A., Sparks, R., Lassey, K. R., and Riedel, K. (2011). Tropospheric <sup>14</sup>CO<sub>2</sub> at wellington, new zealand: the world’s longest record. *Biogeochemistry*, 104(1):5–22.
- Graven, H. D. (2015). Impact of fossil fuel emissions on atmospheric radiocarbon and various applications of radiocarbon over this century. *Proceedings of the National Academy of Sciences*, 112(31):9542–9545.
- Graven, H. D., Guilderson, T. P., and Keeling, R. F. (2012). Observations of radiocarbon in CO<sub>2</sub> at seven global sampling sites in the Scripps flask

- network: Analysis of spatial gradients and seasonal cycles. *Journal of Geophysical Research: Atmospheres*, 117(D2). D02303.
- Hertelendi, E. and Csongor, E. (1983). Anthropogenic  $^{14}\text{C}$  excess in the troposphere between 1951 and 1978 measured in tree rings. *Radiochemical and Radioanalytical letters*, 56(2):103–110.
- Hsueh, D. Y., Krakauer, N. Y., Randerson, J. T., Xu, X., Trumbore, S. E., and Southon, J. R. (2007). Regional patterns of radiocarbon and fossil fuel-derived  $\text{CO}_2$  in surface air across North America. *Geophysical Research Letters*, 34(2):n/a–n/a. L02816.
- Hua, Q. and Barbetti, M. (2004). Review of tropospheric bomb  $^{14}\text{C}$  data for carbon cycle modeling and age calibration purposes. *Radiocarbon*, 46(3):1273–1298.
- Hua, Q., Barbetti, M., Jacobsen, G., Zoppi, U., and Lawson, E. (2000). Bomb radiocarbon in annual tree rings from Thailand and Australia. *Nuclear Instruments and Methods in Physics Research Section B: Beam Interactions with Materials and Atoms*, 172(1):359 – 365. 8th International Conference on Accelerator Mass Spectrometry.
- Hua, Q., Barbetti, M., Levchenko, V. A., D’Arrigo, R. D., Buckley, B. M., and Smith, A. M. (2012). Monsoonal influence on southern hemisphere  $^{14}\text{CO}_2$ . *Geophysical Research Letters*, 39(19). L19806.
- Hua, Q., Barbetti, M., and Rakowski, A. (2013). Atmospheric radiocarbon for the period 1950–2010. *Radiocarbon*, 55(4):2059–2072.

- Hyndman, A. R., Koehler, A., Ord, K., and Snyder, R. (2008). *Forecasting with Exponential Smoothing*. Springer Series in Statistics. Springer Berlin Heidelberg.
- Hyndman, R. J. and Khandakar, Y. (2008). Automatic time series forecasting: The forecast package for R. *Journal of Statistical Software*, 27(3):1–22.
- Levin, I. and Kromer, B. (1997). Twenty years of atmospheric  $^{14}\text{CO}_2$  observations at Schauinsland station, Germany. *Radiocarbon*, 39(2):205–218.
- Levin, I. and Kromer, B. (2004). The tropospheric  $^{14}\text{CO}_2$  level in mid-latitudes of the northern hemisphere (1959–2003). *Radiocarbon*, 46(3):1261–1272.
- Levin, I., Kromer, B., and Hammer, S. (2013). Atmospheric  $\Delta^{14}\text{CO}_2$  trend in Western European background air from 2000 to 2012. *Tellus B*, 65(0).
- Levin, I., Naegler, T., Kromer, B., Diehl, M., Francey, R. J., Gomez-Pelaez, A. J., Steele, L. P., Wagenbach, D., Weller, R., and Worthy, D. E. (2010). Observations and modelling of the global distribution and long-term trend of atmospheric  $^{14}\text{CO}_2$ . *Tellus B*, 62(1):26–46.
- Levin, I., Schuchard, J., Kromer, B., and Muennich, K. (1989). The continental European Suess effect. *Radiocarbon*, 31(3):431–440.
- Manning, M. R., Lowe, D. C., Melhuish, W. H., Sparks, R. J., Wallace, G., Brenninkmeijer, C. A. M., and McGill, R. C. (1990). The use of radiocarbon measurements in atmospheric studies. *Radiocarbon*, 32(1):37–58.

- Meijer, H. A. J., Pertuisot, M. H., and van der Plicht, J. (2006). High-accuracy  $^{14}\text{C}$  measurements for atmospheric  $\text{CO}_2$  samples by AMS. *Radiocarbon*, 48(3):355–372.
- Naegler, T. and Levin, I. (2006). Closing the global radiocarbon budget 1945–2005. *Journal of Geophysical Research: Atmospheres*, 111(D12):n/a–n/a. D12311.
- Nijman, T. E. and Palm, F. C. (1990). Predictive accuracy gain from disaggregate sampling in ARIMA models. *Journal of Business & Economic Statistics*, 8(4):405–415.
- Nydal, R. and Loevseth, K. (1996). *Carbon-14 Measurements in Atmospheric  $\text{CO}_2$  from Northern and Southern Hemisphere Sites, 1962-1993*. Oak Ridge National Laboratory.
- Oeschger, H., Siegenthaler, U., Schotterer, U., and Gugelmann, A. (1975). A box diffusion model to study the carbon dioxide exchange in nature. *Tellus*, 27(2):168–192.
- Park, J. H., Kim, J. C., Cheoun, M. K., Kim, I. C., Youn, M., Liu, Y. H., and Kim, E. S. (2002).  $^{14}\text{C}$  level at Mt Chiak and Mt Kyeryong in Korea. *Radiocarbon*, 44(2):559–566.
- Rakowski, A. Z., Nadeau, M.-J., Nakamura, T., Pazdur, A., Pawełczyk, S., and Piotrowska, N. (2013). Radiocarbon method in environmental monitoring of  $\text{CO}_2$  emission. *Nuclear Instruments and Methods in Physics Research Section B: Beam Interactions with Materials and Atoms*, 294:503

- 419 – 507. Proceedings of the Twelfth International Conference on Accelerator  
420 Mass Spectrometry, Wellington, New Zealand, 20-25 March 2011.
- 421 Randerson, J. T., Enting, I. G., Schuur, E. A. G., Caldeira, K., and Fung,  
422 I. Y. (2002). Seasonal and latitudinal variability of troposphere  $\Delta^{14}\text{CO}_2$ :  
423 Post bomb contributions from fossil fuels, oceans, the stratosphere, and  
424 the terrestrial biosphere. *Global Biogeochemical Cycles*, 16(4):59–1–59–19.
- 425 Reimer, P., Brown, T., and Reimer, R. (2004). Reporting and calibration of  
426 Post-Bomb  $^{14}\text{C}$  data. *Radiocarbon*, 46(3).
- 427 Rossana, R. J. and Seater, J. J. (1995). Temporal aggregation and economic  
428 time series. *Journal of Business & Economic Statistics*, 13(4):441–451.
- 429 Sierra, C. A., Müller, M., and Trumbore, S. E. (2014). Modeling radiocarbon  
430 dynamics in soils: SoilR , version 1.1. *Geosci. Model Dev.*, 7(7):1919–1931.  
431 GMD.
- 432 Steinhof, A., Adamiec, G., Gleixner, G., Wagner, T., and van Klinken, G.  
433 (2004). The new  $^{14}\text{C}$  analysis laboratory in Jena, Germany. *Radiocarbon*,  
434 46(1):51–58.
- 435 Suess, H. E. (1953). Natural radiocarbon and the rate of exchange of carbon  
436 dioxide between the atmosphere and the sea. In *Nuclear Processes in*  
437 *Geological Settings*, pages 52–56. National Research Council Publications.
- 438 Suess, H. E. (1955). Radiocarbon concentration in modern wood. *Science*,  
439 122(3166):415–417.

- 440 Synal, H.-A., Stocker, M., and Suter, M. (2007). MICADAS: A new compact  
441 radiocarbon AMS system. *Nuclear Instruments and Methods in Physics  
442 Research Section B: Beam Interactions with Materials and Atoms*, 259(1):7  
443 – 13. Accelerator Mass Spectrometry.
- 444 Tans, P. P., de Jong, A. F. M., and Mook, W. G. (1979). Natural atmospheric  
445  $^{14}\text{C}$  variation and the Suess effect. *Nature*, 280(5725):826–828.
- 446 Turnbull, J., Rayner, P., Miller, J., Naegler, T., Ciais, P., and Cozic, A.  
447 (2009). On the use of  $^{14}\text{CO}_2$  as a tracer for fossil fuel  $\text{CO}_2$ : Quantifying  
448 uncertainties using an atmospheric transport model. *Journal of Geophys-  
449 ical Research: Atmospheres*, 114(D22). D22302.
- 450 Turnbull, J. C., Lehman, S. J., Miller, J. B., Sparks, R. J., Southon, J. R.,  
451 and Tans, P. P. (2007). A new high precision  $^{14}\text{CO}_2$  time series for North  
452 American continental air. *Journal of Geophysical Research: Atmospheres*,  
453 112(D11). D11310.
- 454 Vogel, J. C. and Marais, M. (1971). Pretoria radiocarbon dates i. *Radiocar-  
455 bon*, 13(2):378–394.
- 456 Wacker, L., Bonani, G., Friedrich, M., Hajdas, I., Kromer, B., Němec, M.,  
457 Ruff, M., Suter, M., Synal, H.-A., and Vockenhuber, C. (2010). Micadas:  
458 Routine and high-precision radiocarbon dating. *Radiocarbon*, 52(2):252–  
459 262.
- 460 Yamada, Y., Yasuike, K., and Komura, K. (2005). Temporal variation of  
461 carbon-14 concentration in tree-ring cellulose for the recent 50 years. *Jour-  
462 nal of Nuclear and Radiochemical Sciences*, 6(2):135–138.

## 463 Figure captions

Figure 1: Atmospheric radiocarbon curves obtained by Hua et al. (2013). a) Original data for four different atmospheric regions, b) time series constructed from original data for the period 1975 to 2010.

Figure 2: Trend (level and slope) and seasonality of the atmospheric radiocarbon time series predicted by the best-fit model for the hemispheric series compiled by Hua et al. (2013). For both series, the best model selected based on the AIC was an ETS model of the form (M,A,M), i.e. a multiplicative term for the error, an additive term for the trend, and a multiplicative term for the seasonality.

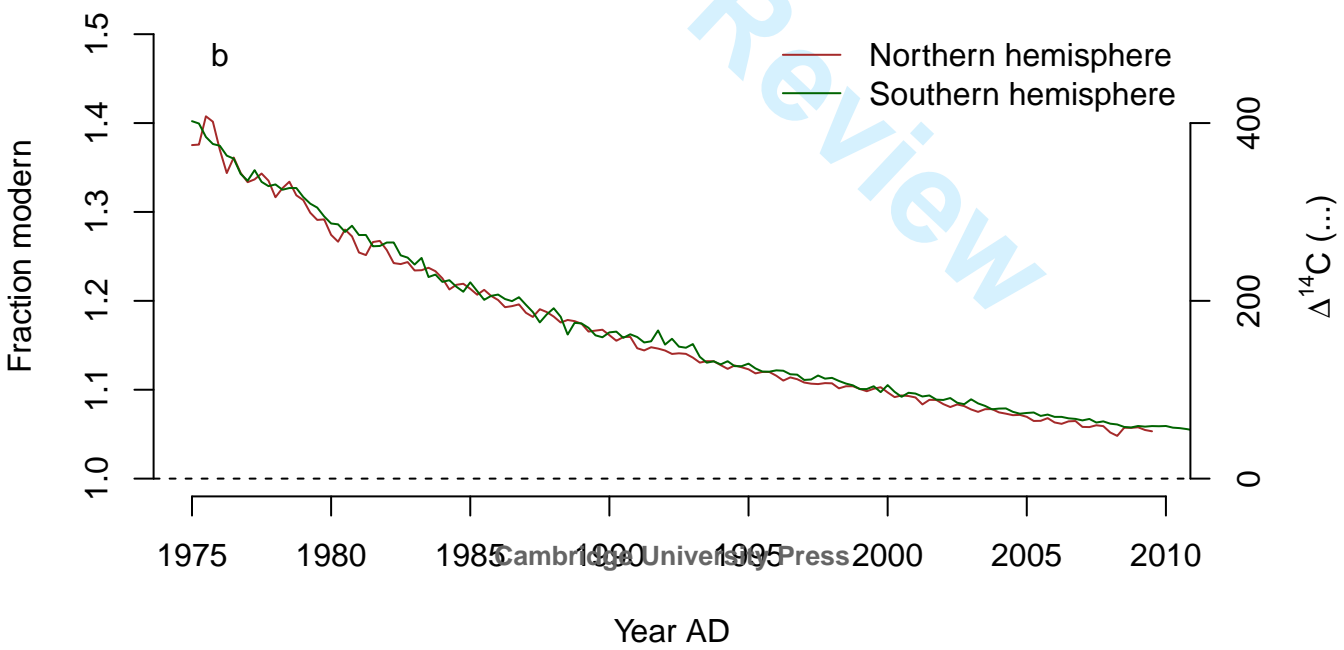
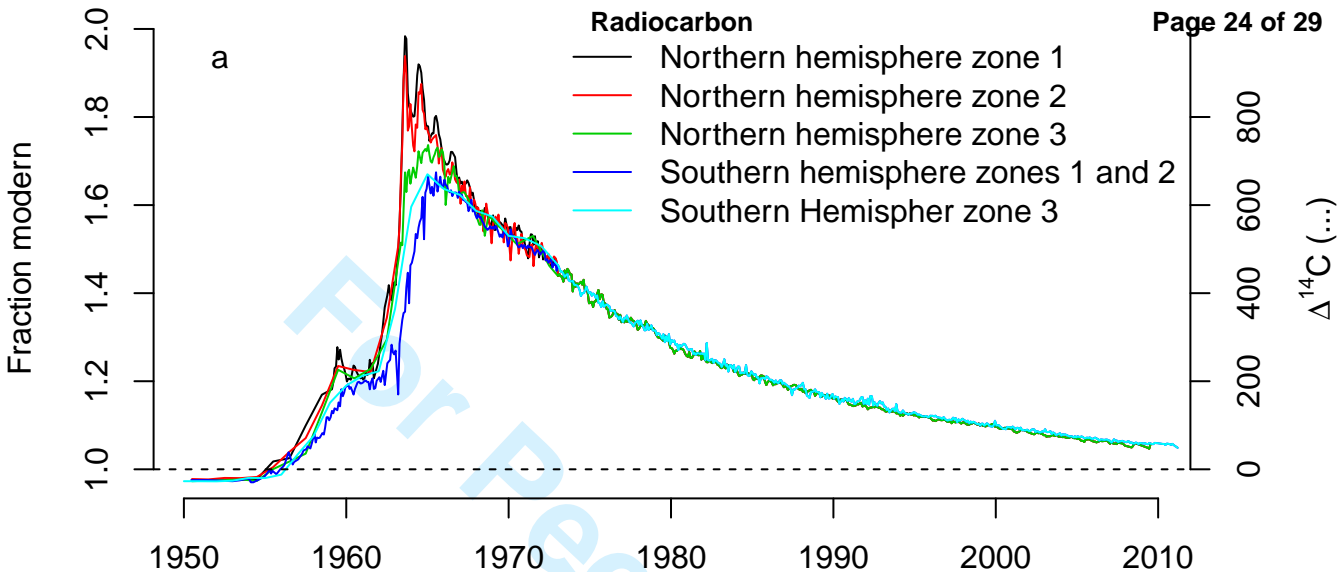
Figure 3: Forecast of atmospheric radiocarbon for the northern and southern hemispheres based on the best ETS model. Shaded regions in gray and blue show the 95 and 80% prediction intervals.

Figure 4: a) Forecast (with 80 and 95% prediction intervals) for the northern hemisphere radiocarbon curve compared to observations at the Jungfraujoch and Schauinsland reported in Levin et al. (2013). b) Optimized forecast for central Europe forcing the model to pass through the observations from these two stations.

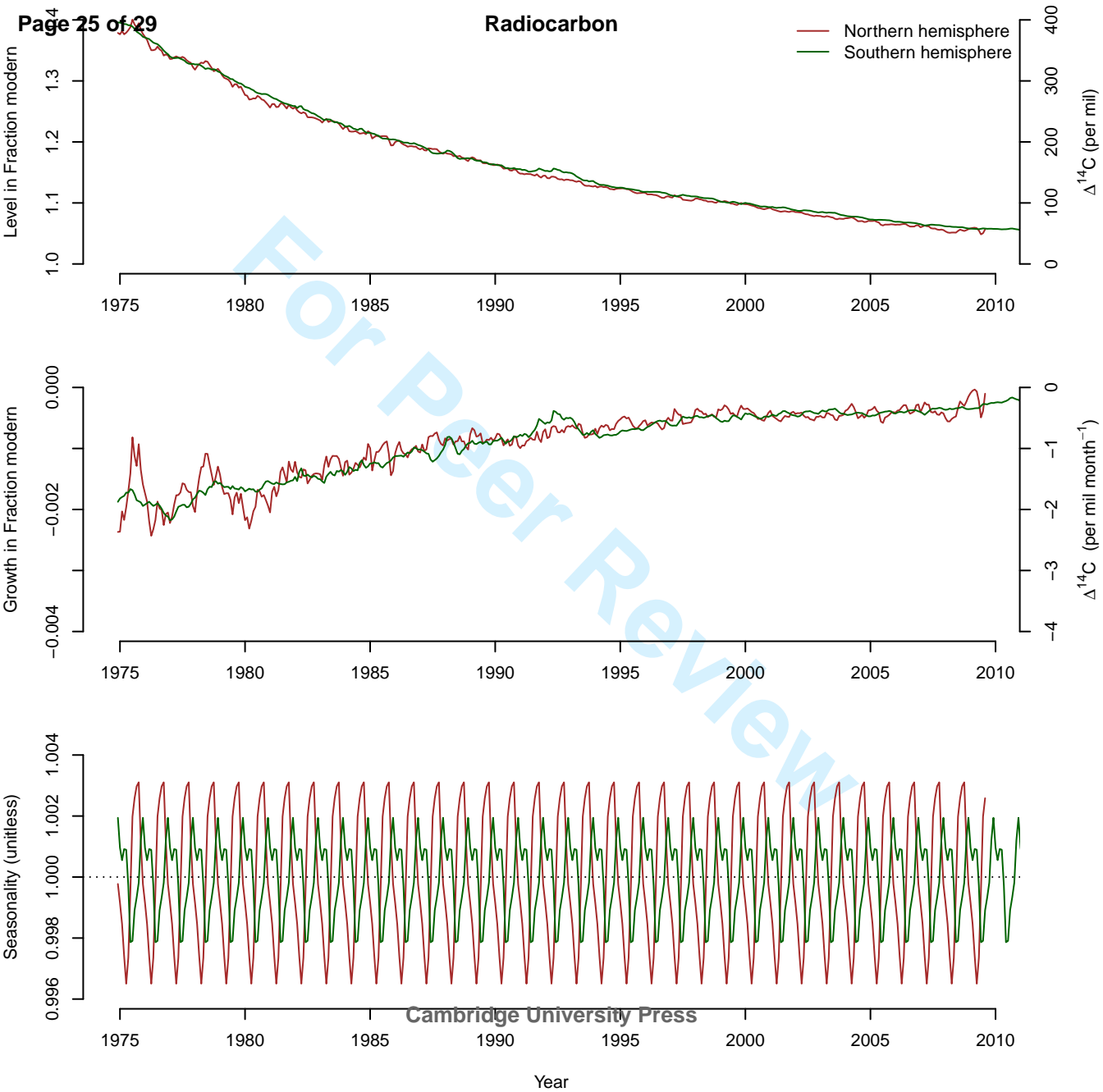
Figure 5: Probability of  $\Delta^{14}\text{C} \leq 0\text{‰}$  for the different hemispheric zones calculated as 100 minus different probability levels of the lower prediction interval for each forecast time. As a reference, 20 and 5% probability levels are presented in dashed and dotted lines, respectively. The vertical dotted line represents July 2017.

Figure 6: Forecasted northern hemisphere atmospheric radiocarbon concentrations (with 80 and 95% prediction intervals), superimposed with radiocarbon concentration measured in plants growing on different industrial cities and remote areas without fossil fuel influence. This radiocarbon concentration represents the mix of fossil-fuel derived carbon and the mixing with background air.

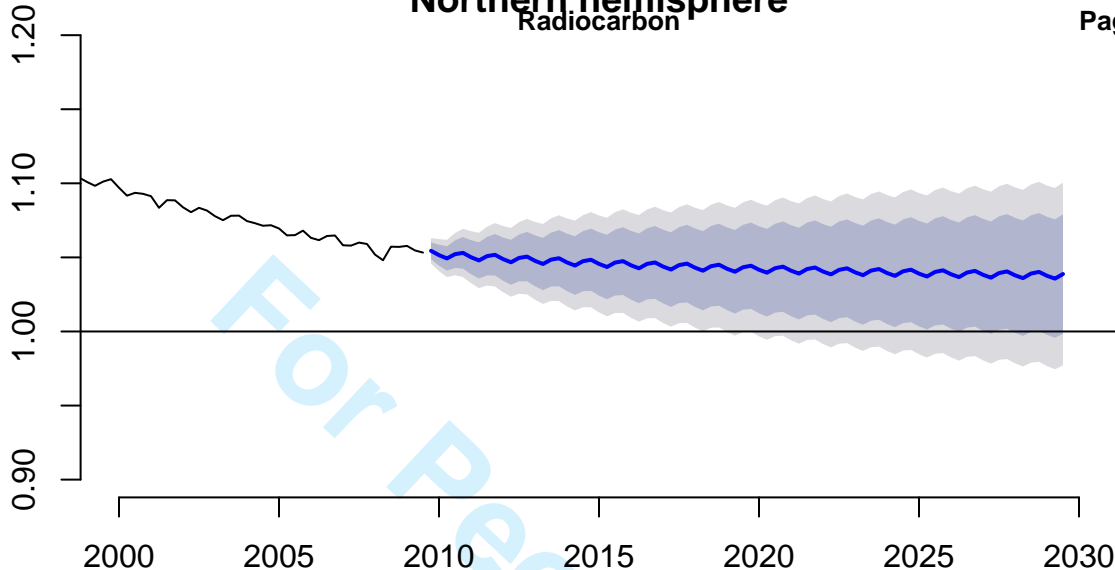




## Radiocarbon

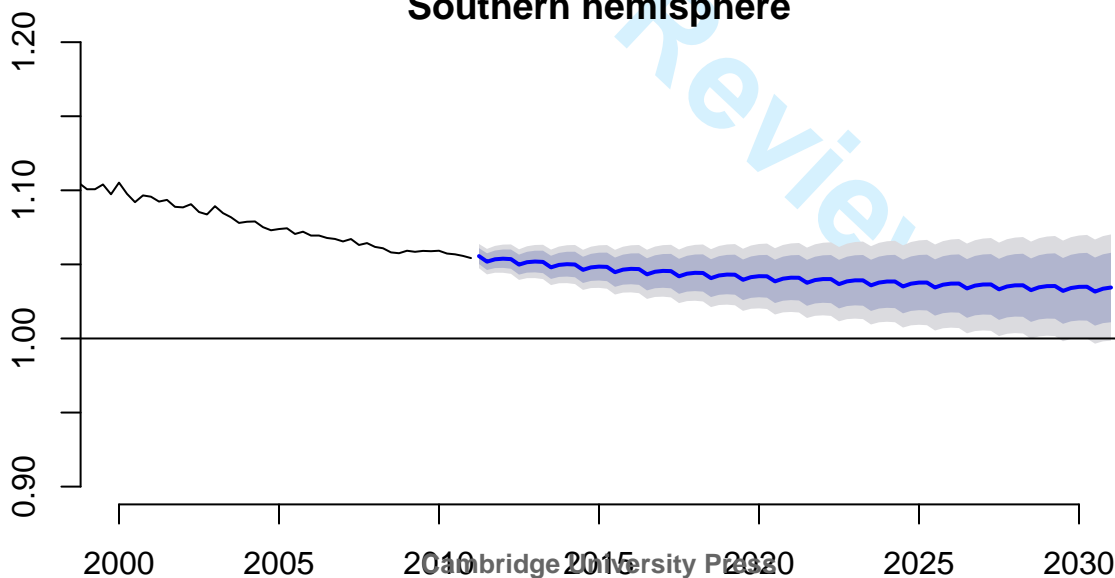


Fraction modern



## Southern hemisphere

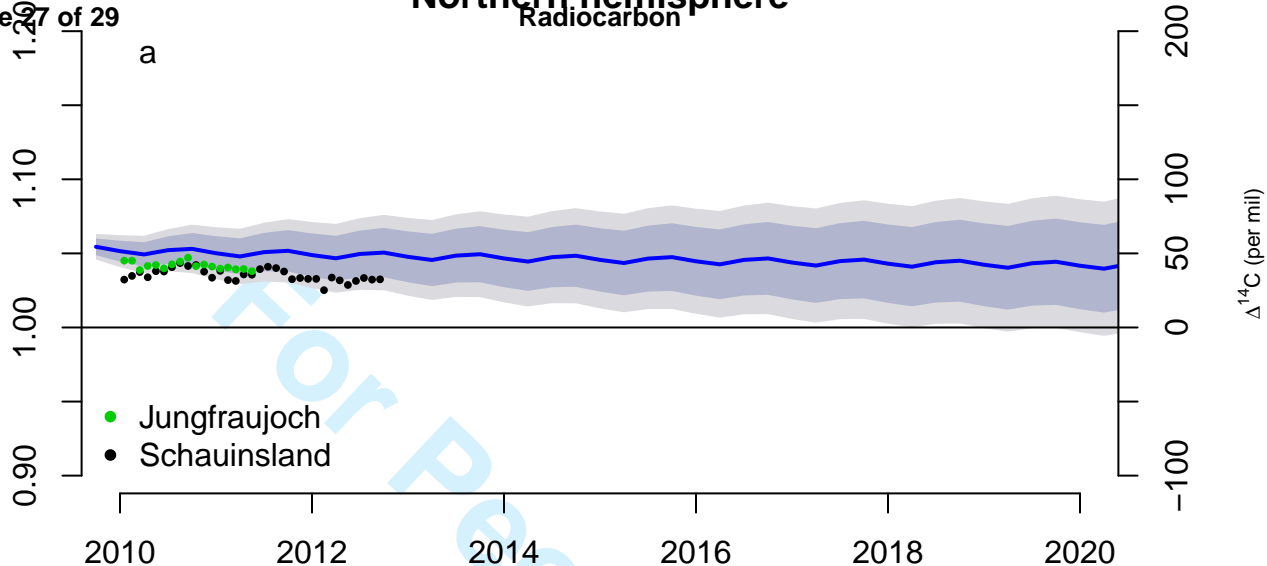
Fraction modern



Year

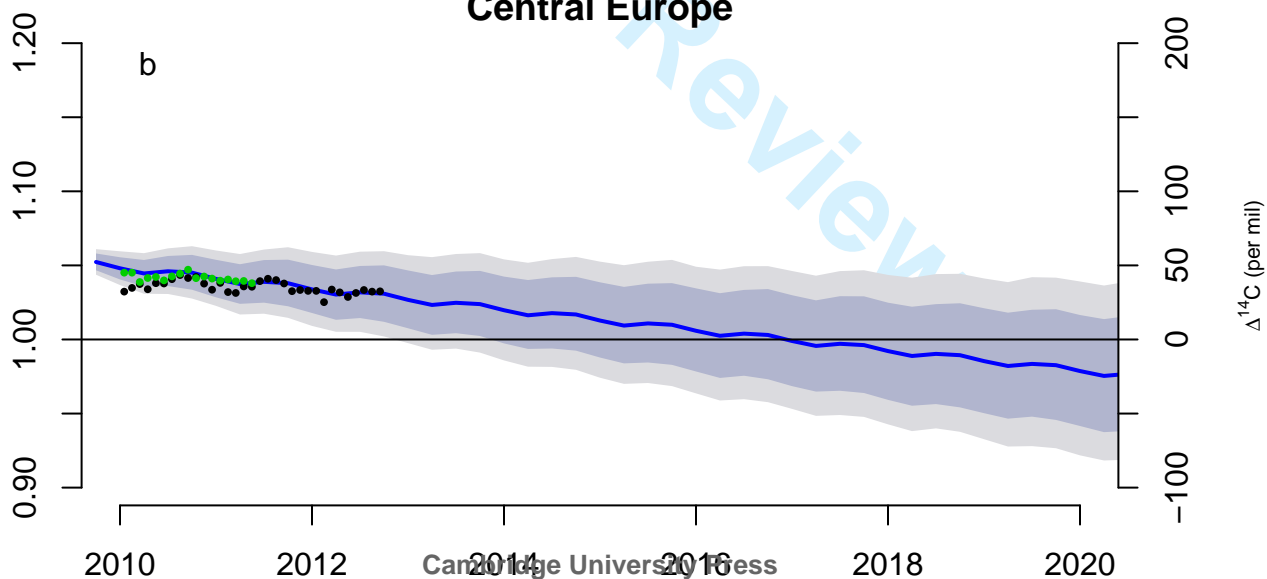
Northern hemisphere  
Radiocarbon

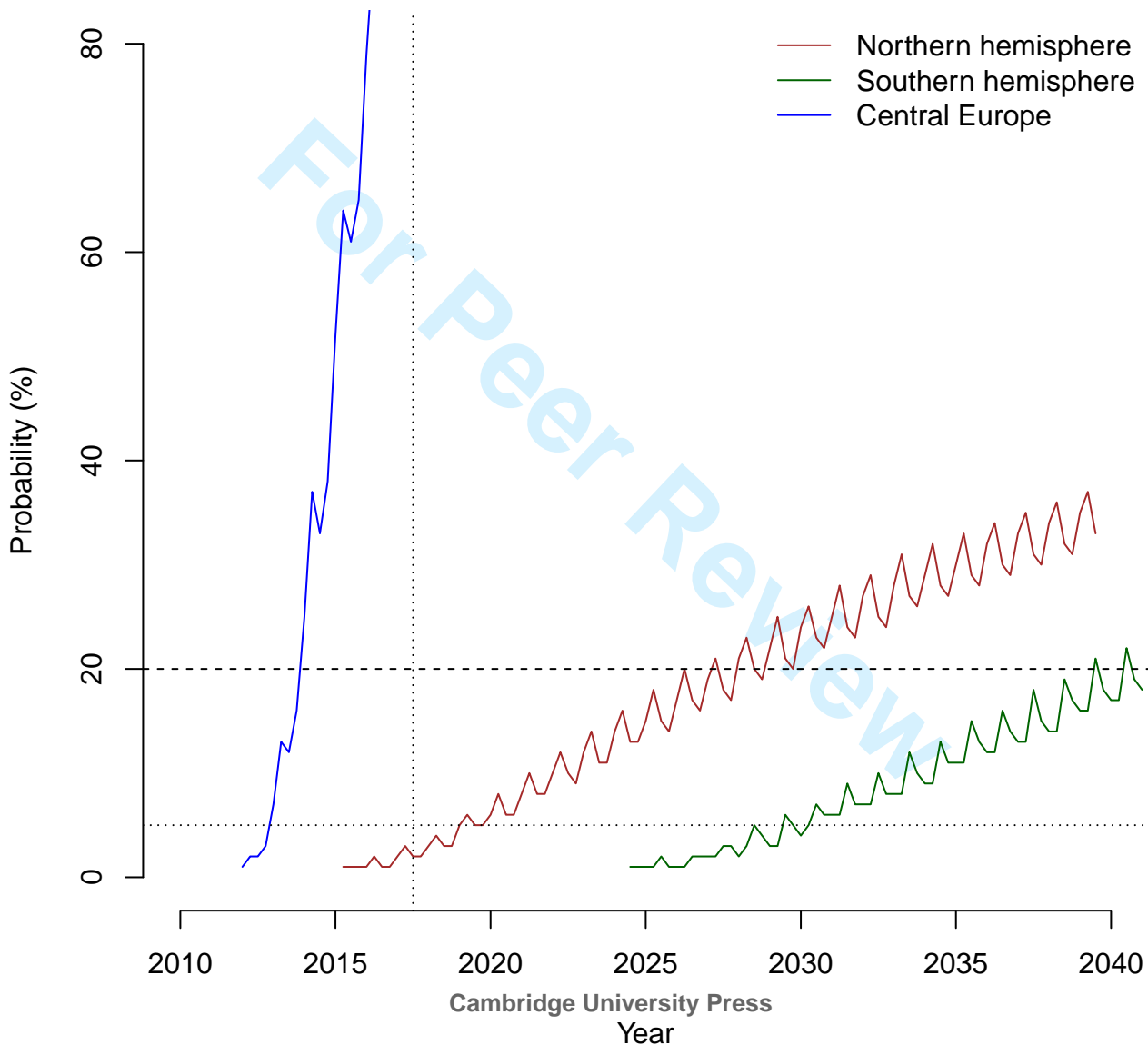
Fraction modern



## Central Europe

Fraction modern





Fraction modern

